International Journal of Current Engineering and Technology
E-ISSN 2277 – 4106, P-ISSN 2347 - 5161

Available at http://inpressco.com/category/ijcet

Research Article

Rim Stress Analysis of Epicyclic Gearbox

Mahendra Kalyanshetti[Á*], Suresh Wadkar[Á] and Sateesh Patil[Á]

[Á]Mechanical Department, Pune University, Pune, Maharashtra, India

Accepted 10 July 2014, Available online 01 Aug 2014, **Vol.4, No.4 (Aug 2014)**

Abstract

The design procedures developed for external gear pairs are often used for planetary gears. The gear rims of external as well as particularly ring gear are thin in case of planetary gear box. The thin rims are preferred because of cost reduction and weight reduction also. Therefore rim stresses become important for these types of gear boxes. In this paper rim stress for a ring gear are estimated by using curved beam theory. The bending stresses and the stresses across the thickness of ring gear are also estimated by Finite element Method (FEM). The experimental setup consists of planetary gear box with strain gauges mounted on the rim of ring gear. The stress measurement is done under static loading conditions, for which output shaft was locked with suitable locking arrangement. The input torque was provided with a lever attached to the input shaft. The experimental stresses on the rim surface for different planet positions were compared with FEM results. The stresses across the rim thickness are estimated with FEM and are in good agreement with the theoretical. The effect of angular position of planet on the root stress of ring gear is evaluated. The stress distribution along the length of rim between two fixing bolts is estimated by FEM.

Keywords: *Epicyclic Gearbox, Rim Stress, Finite Element Analysis, Ring Gear*

1. Introduction

Epicyclic gear train is a gearing system consisting of one or more ring gears, or planet gears, revolving about a central, or sun gear. The planet gears are mounted on a movable arm or carrier which itself may rotate relative to the sun gear. Epicyclic gearing systems also incorporate the use of ring gear or annulus, which meshes with the planet gears. The rim thickness of the internal gear is a key parameter that must be defined carefully in order to meet certain design objectives regarding power density, load sharing, noise and durability. The rim of the internal gear must be as thin as possible in order to maximize the power density and minimize mass. For a typical automotive automatic transmission planetary gear set, a 1 mm reduction of rim thickness of an internal gear may result up to 20 percent reduction in mass of the internal gear, which is rather significant. Besides reducing mass, added i flexibility through reduced rim thickness offers a number of functional improvements to the planetary gear set.

A theoretical method of obtaining the nominal stress in the rim of planet gear with both a thin rim and clearance between the rim and gear shaft is shown by using an equivalent ring. In the analysis, the boundary position between the region where the rim is in contact with the shaft and that where they are out of contact with each other is assumed because the boundary condition depends on the tooth load and clearance in case of constant rim thickness. Using the true boundary position, the bending moment and the circumferential forces in the rim are obtained by Takeshi Ishida et al. (1986). The comparative analysis of tooth-root strength evaluation methods used within ISO and AGMA standards and verifying them with developed models and simulations using the finite element method (FEM) is done. The analysis for various combinations of design, manufacturing and performance parameters are illustrated graphically and discussed briefly by Andrzej Kawalec et al. (2006). M. Rameshkumar (2010) explained finite element analysis of high contact ratio HCR, normal contact ratio NCR gears with same module, centre distance and the comparison of bending, contact stress for both HCR, NCR gears. A two dimensional deformable body contact model of HCR and NCR gears is analyzed using ANSYS software. The variation of gear mesh stiffness for HCR gears is less than the normal contact ratio (NCR) gears; the transmission error for HCR gears is minimum compared to NCR gears. Niels L. Pedersen et al. (2010) explained that the bending stress is indirectly related to the shape changes by the cutting tool. It shows that the bending stress can be reduced significantly by using asymmetric gear teeth and by shape optimizing the gear through changes made to the tool geometry. The cutting tool is designed so that root shape optimization of the gear tooth is achieved and it is directly related to the actual gear tooth. The reduction in the bending stress is about 44.3% as compare to normal gear tooth profile. Shuting Li et al (2008), established an effect of addendum on tooth contact strength, bending strength and basic performance parameters of spur gears. Face-contact model of teeth, mathematical programming

*Corresponding author: **Mahendra Kalyanshetti**

Table 1 Specifications of Epicyclic Gearbox

Parameter	Sun gear	Planet Gears	Ring gear
Number of teeth	10	19	50
Module (mm)	3.25	3.25	3.25
Pressure angle (deg)	20^0	20^0	20^0
Diameter of pitch circle (mm)	35.75	63.38	162.50
Root Diameter (mm)	27.62	55.25	170.62
Outer Diameter (mm)	42.25	69.88	156.00
Face width (mm)	31	30	31
Young's modulus (MPa)	2.05×10^5	2.05×10^5	2×10^5
Poisson's ratio	0.29	0.29	0.29
Material	SAE 8620	SAE 8620	EN8/AISI1040
Density (kg/m^3)	7850	7850	7845
Yield Strength (N/mm^2)	833	833	415

method and three-dimensional, FEM are used together to conduct loaded tooth contact analyses, deformation and stress calculations of spur gears with different addendums and contact ratios. Tooth load, load-sharing rate, contact stress, root bending stress, transmission error and mesh stiffness of the spur gears are analyzed. The maximum contact stress is also not exactly at the geometrical contact point. Hertz formula can only calculate the tooth contact stress approximately. FEM can be used to conduct precise analysis of the tooth contact stress. It is also found that increment of addendum can increase number of contact teeth, then this increment can reduce tooth contact stress and root bending stress.

In this paper rim stresses for a ring gear are estimated by using curved beam theory. The root stresses and the stresses across the thickness of ring gear are also estimated by Finite element Method (FEM). The experimental setup consists of planetary gear box with strain gauges mounted on the rim of ring gear. The stress measurement is done under static loading conditions, for which output shaft was locked with suitable locking arrangement.

2. Modeling of Epicyclic Gear Train

Involute spur gears are the most common form of gears which are used to transfer the motion between the parallel shafts.

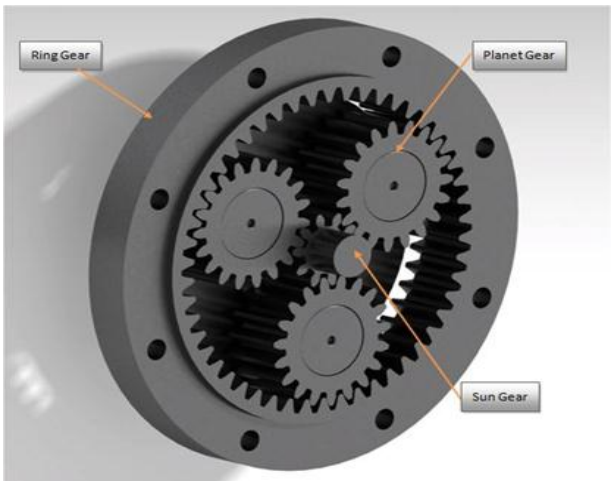

Fig.1. CATIA model of Epicyclic gear train

The main concerns while designing an involute spur gear include generation of involute. In earlier days to design an involute spur gear there were many theoretical procedures to draw an approximate involute but no procedure was present to draw a perfect involute for performing analysis. In the present day with the 3-D modeling software's it is easy to generate the involute spur gear with exact involute. In this paper, the involute spur gear with perfect involute is generated in CATIA V5R19 as shown in Fig.1. The specifications of epicyclic gear box are given in Table.1.

3. Theoretical Stress Formulae

The force distribution in complete epicyclic gear train is as shown in Fig. 2 in which the input torque is applied on the sun gear in clockwise direction causes the sun gear rotates about its centre. While planet gears are revolving about the sun gear in anticlockwise direction or vice versa when the ring gear is fixed. The carrier is used to hold the planet gear through pins and produce output of the gear box in anticlockwise direction.

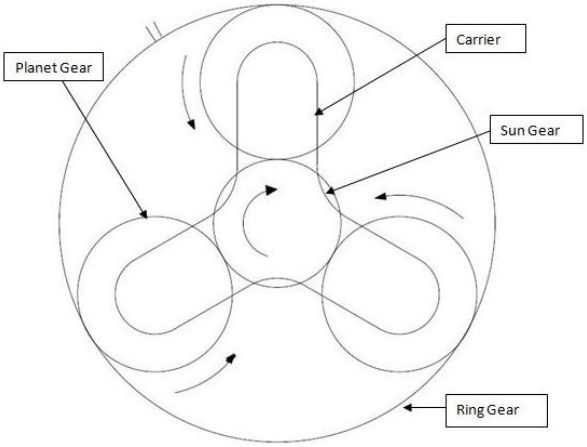

Fig. 2 Simple epicyclic gear train

Fig. 3 shows the free body diagram of complete epicyclic gear train in which the input torque is applied to the sun gear. The resultant forces on the gear tooth are resolve into two components namely tangential force and radial force. In which the tangential force causes bending stresses on

the gear tooth and radial force produces the compressive stresses on the gear .The sun gear is engaged to the three planet gears which are 120° apart from each other, therefore these resolved component is applied on each planet gear. The planet gear meshes with the sun gear and ring gear which produces two tangential forces, therefore twice the tangential force is require to hold the planet gear.

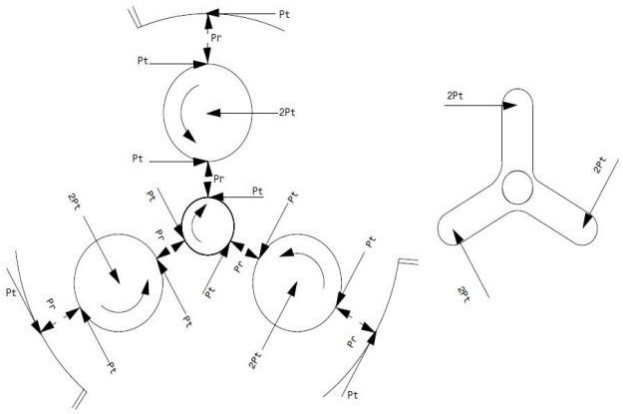

Fig. 3 Free body diagram of complete epicyclic gear train

3.1 Rim Stresses

The main failure modes in planetary gear sets are associated with gear tooth bending fatigue, ring gear hoop fatigue, pitting due to contact fatigue and planet bearing fatigue. The meshes of the planetary gear sets are often designed individually by using procedures developed for typical external gear pairs. This poses several complications since there are a number of system-level factors that are unique to planetary gear sets.

Derivation of Bending stresses in ring gear

It is assumed that the centre line of the bar is a plane curve and that the cross sections have an axis of symmetry in this plane. The bar is subjected to the action of force lying in this symmetry. The bar of constant cross section is in pure bending due to couples applied at the ends as shown in Fig. 4.

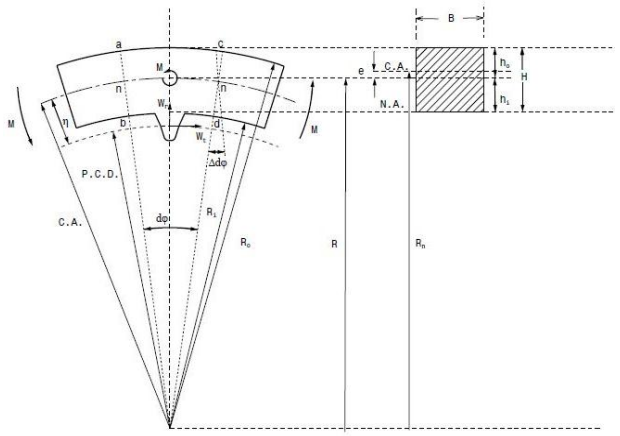

Fig. 4 Specifications of Cut section of ring gear

Let *ab* and *cd* denote two neighbouring cross sections of the bar and let $d\varphi$ denote the small angle between them before bending. As a result of bending, the cross section *cd* rotates with respect to *ab*. Let $\Delta d\varphi$ denotes the small angle of rotation. Due to this rotation the longitudinal fibers on the convex side of the bar are compressed and the fibers on the concave side of the bar are extended.

If n-n denotes the neutral surface, the extension of any fiber at distance y from this surface is $y\Delta d\varphi$ and the corresponding unit elongation is

$$\epsilon = \frac{y\Delta d\varphi}{(r-y)d\varphi} \quad (1)$$

Where,
$d\varphi$ = small angle between neighbouring cross sections before bending.
$\Delta d\varphi$ = small angle of rotation.
ϵ = unit elongation.
r = radius of the neutral surface.
y = extension of any fiber from neutral axis.

Where r denotes the radius of the neutral surface and the denominator in eq. 1 is the length of the fiber between the adjacent cross sections before bending. Assuming that there is no lateral pressure between the longitudinal fibers, the bending stress at a distance y from the neutral axis is

$$\sigma_x = \frac{Ey\Delta d\varphi}{(r-y)d\varphi} \quad (2)$$

Where
σ_x = bending stress.
E = young's modulus.

It will be seen that the stress distribution is no longer linear as in case of straight bars, but that follows a hyperbolic law. From the condition that the sum of the normal forces distributed over the cross section is zero, it can be concluded that the neutral axis is displaced from the centroid of the cross section towards the center of the curvature of the bar. In order to have the stresses in the most remote fiber in tension and compression equal, it is necessary to use sectional shapes which have the centroid nearer the concave side of the bar.

Eq. (2) contains two unknowns, the radius r of the neutral surface and the angle $\Delta d\varphi$ which represents the angular displacement due to bending. To determine them we must use the two equations of statics. The first equation is based on the condition that the sum of the normal forces distributed over the cross section is equal to zero. The second equation is based on the condition that the moment of these normal forces is equal to the bending moment M. These equations are:

$$\int \sigma_x \, dA = \frac{E\Delta d\varphi}{d\varphi} \int \frac{ydA}{r-y} = 0 \quad (3)$$

$$\int \sigma_x \, ydA = \frac{E\Delta d\varphi}{d\varphi} \int \frac{y^2 dA}{r-y} = M \quad (4)$$

Where,
M = bending moment

A = cross sectional area

The integration in both equations is extended over the total area of the cross section. The integral in eq. (4) may be simplified as follows:

$$\int \frac{y^2 dA}{r-y} = -\int \left(y - \frac{ry}{r-y}\right) dA \quad (5)$$

$$\int \frac{y^2 dA}{r-y} = -\int \left(y - \frac{ry}{r-y}\right) dA = -\int y dA + r\int \frac{y dA}{r-y} \quad (6)$$

The first integral on the right side of eq.(6) represents the moment of the cross sectional area with respect to the neutral axis and second, as is seen from eq.(3), is equal to zero. Hence

$$\int \frac{y^2 dA}{r-y} = Ae\,, \quad (7)$$

In which e denotes the distance of the neutral axis from the cendroid of the cross section. Equation (4) then becomes

$$\frac{E\Delta d\varphi}{d\varphi} = \frac{M}{Ae} \quad (8)$$

And equation (8) gives

$$\sigma_x = \frac{My}{Ae(r-y)} \quad (9)$$

The stresses in the most remote fibers, which are the maximum stresses in bar are

$$\boldsymbol{\sigma_{max}} = \frac{\boldsymbol{M*h_i}}{\boldsymbol{A*e*R_i}}$$

$$\boldsymbol{\sigma_{min}} = \frac{\boldsymbol{M*h_o}}{\boldsymbol{A*e*R_o}} \quad (10)$$

Where,
M = Bending Moment w.r.to centroidal axis
h_i= Distance of inner fiber from Neutral axis
h_o= Distance of outer fiber from Neutral axis
A = Cross sectional area
e = Eccentricity between centroidal and neutral axis
Where
$M = W_t * \eta$
Where
W_t = Tangential force (N)
η = Radial distance between pitch circle diameter and Neutral axis
$e = R - R_N$
Where

$$R_N = \frac{h}{\log_e\left(\frac{R_o}{R_i}\right)}$$

And

$$R = R_i + \frac{h}{2}$$

Where,
R = Radius of centroidal axis
R_N = Radius of neutral axis
R_i = Inner rim radius
R_o =Outer rim radius
h = Thickness of rim
b = Width of rim

4. Experimental Setup

For static analysis, loading arrangement is used to apply the input torque to the sun gear by changing the weight, instead of providing the input torque from the motor. The loading of gear box is made with the help of a lever of 595mm in length on one side of which a pan is attached for the purpose of addition of weights, while the other end is having a key slot which can be fitted in the input shaft of the gear box. This results in providing the input torque to the sun gear as shown in Fig.5.

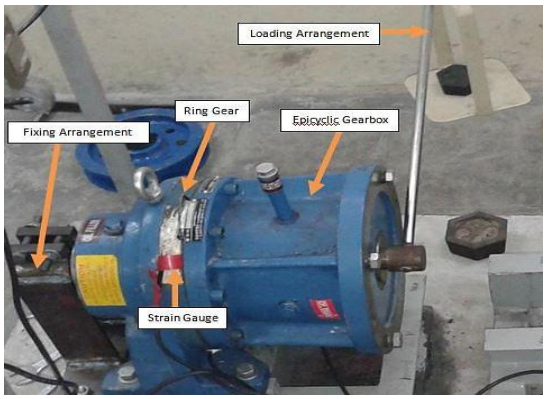

Fig. 5 Experimental Setup

As shown in Fig.5, the output shaft is fixed with the help of a fixture. For static analysis fixing arrangement is used instead of dynamometer to fix the output shaft i.e. to fix the carrier. In this fixture a hub is welded with two vertical plates of same dimensions, these plates then welded to the horizontal plate which in turn fixed to the frame of the set up with bolts. A hub can be loosened or tightened with the help of nut and bolts. The main reason to make this fixing arrangement is to lock the output shaft at the desired position to avoid slipping during the loading.

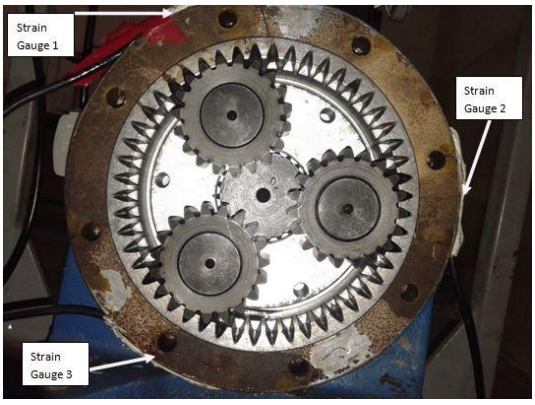

Fig. 6 Strain Gauge Location

Strain gauges are mounted on the outer surface of the ring gear to measure the hoop stresses. The ring gear is fixed

with the help of eight bolts to the gear box casing. Fig.6 shows the location of strain gauges on the outer surface of the ring gear which are 120° away from each other. The locations of strain gauges are preferred where planet gear meshes to the ring gear which produces maximum hoop stresses.

5. Finite Element Analysis Procedure

Finite Element analysis for any 3-D model is performed in three main steps namely Pre-Processing, Solution, Post-Processing.

5.1 Pre-Processing

The Pre-Processing mainly involves the modeling of the 3-D part. The main steps in Pre-Processing are Engineering Data, Geometry and Discretization.

The gear geometry generated from CATIA is imported in to Ansys workbench through Design Modeler.

Discretization is the method of converting continuous models to discrete parts. The goal is to select and locate finite element nodes and element types so that the associated analysis is sufficiently accurate. Element Aspect ratio must be near unity to obtain accurate results. For the current analysis average aspect ratio is obtained as 1.85 by setting the mesh relevance to fine and smoothing to medium and span angle center to coarse.

Quadratic elements are used since stress is present all along the thickness of the part. Patch independent algorithm is used since a finer mesh is required around edges and corner. For rest of the body a normal mesh is sufficient and in advanced meshing features the proximity and curvature feature needs to turned on since the curvature size function examines the curvature on the faces and edges and computes the element sizes so that the element size doesn't exceed the maximum size of curvature angle which are either defined by the user or taken automatically. The proximity size function allows defining the minimum number of element layers in the region that constitute gaps. Fig. 7 shows meshing of complete epicyclic gear train which contains 5,57,055 number of nodes and 29,58,149 number of elements.

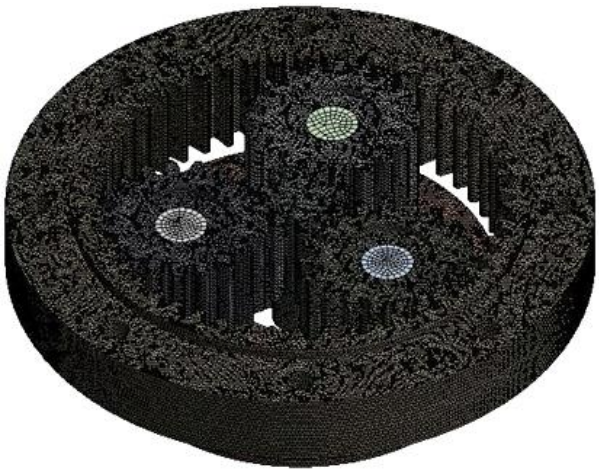

Fig.7 Meshed model of Epicyclic gear train.

5.2. Solution

Solution involves declaration of the analysis type, location of forces and fixation of part as shown in Fig. 8. For the present analysis, the input torque is applied on the sun gear while the ring gear is fixed. The static structural type of analysis is used with no large deflection and inertia relief features. The solver type and weak spring's features are set to program controlled and all the nonlinear controls are turned off. The gear is fixed at the center by the fixed support tool. Forces can be applied to the gear by selecting the edge from the graphics window and forces are defined in the component form.

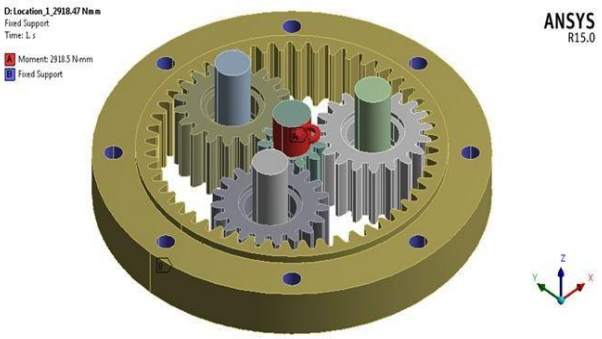

Fig. 8 Boundary Conditions of Epicyclic gear train.

5.3 Post Processing

The post processing stage involves viewing of data files generated by the software during the solution phase. Bending stresses for the gear can be obtained from the maximum principal stresses.

6. Results and Discussion

The experimental setup consists of strain gauges mounted on the outer surface of the ring gear to measure the hoop stresses. The ring gear is fixed with the help of eight bolts to the gear box casing. The location of strain gauges on the outer surface of the ring gear which are 120° away from each other. The locations of strain gauges are preferred where planet gear meshes to the ring gear which produces maximum hoop stresses.

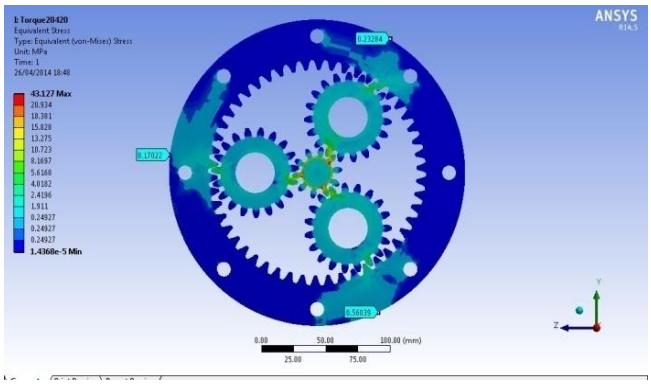

Fig.9 Maximum stresses on ring gear at three different positions

Table 2 Comparison of Ansys and Experimental Stress Results for Outer surface of Ring Gear

S N	Torque(N)	ANSYS Stress Results (N/mm^2)			Experimental Stress Results (N/mm^2)			% of Error		
		Position1	Position 2	Position 3	Position 1	Position 2	Position 3			
1	2910	0.0198	0.0791	0.0195	0.02	0.08	0.02	1.00	1.13	2.20
2	5830	0.0417	0.1580	0.0596	0.04	0.16	0.06	-4.25	1.25	0.67
3	8750	0.0574	0.2380	0.0970	0.06	0.24	0.10	4.33	0.83	3.00
4	11670	0.0955	0.3013	0.1301	0.09	0.30	0.13	-6.11	-0.43	-0.04
5	14590	0.1250	0.4230	0.1702	0.12	0.44	0.17	-4.17	3.86	-0.12
6	17510	0.1441	0.4960	0.1960	0.14	0.50	0.20	-2.93	0.80	2.00
7	20420	0.1702	0.5604	0.2328	0.17	0.56	0.23	-0.12	-0.07	-1.22

Table 3 Experimental rim stresses for 55 deg of rotation

Angle (deg)	Weight (Kg)	Torque (Nmm)	Experimental Stress Results (N/mm^2)		
			Position 1	Position 2	Position3
55	0.500	2910	0.0500	0.2000	0.1500
	1.000	5830	0.1000	0.4000	0.1300
	1.500	8750	0.1300	0.5400	0.1100
	2.000	11670	0.1700	0.7200	0.1000
	2.500	14590	0.1900	0.9400	0.1000
	3.000	17510	0.2000	1.0200	0.1100
	3.500	20420	0.2400	1.1600	0.1100

Table 4 Experimental rim stresses for 60 deg of rotation

Angle(deg)	Weight (Kg)	Torque(Nmm)	Experimental Stress Results (N/mm^2)		
			Position1	Position 2	Position 3
60	0.500	2910	0.02	0.08	0.02
	1.000	5830	0.04	0.16	0.06
	1.500	8750	0.06	0.24	0.10
	2.000	11670	0.09	0.30	0.13
	2.500	14590	0.12	0.44	0.17
	3.000	17510	0.14	0.50	0.20
	3.500	20420	0.17	0.56	0.23

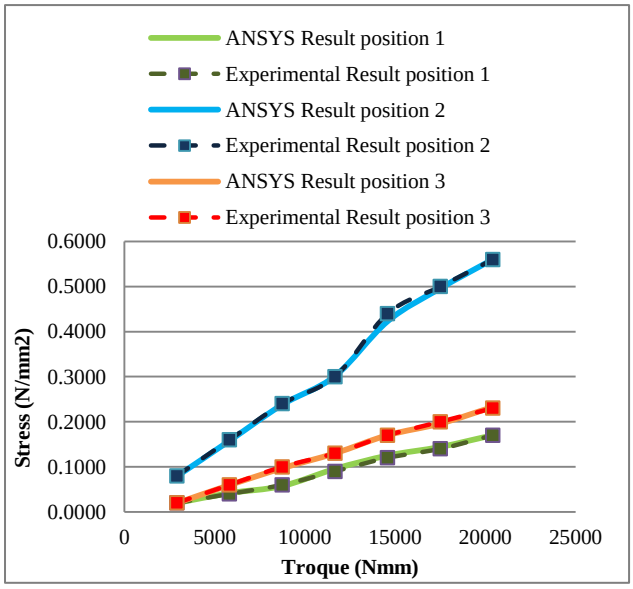

Fig.10 Comparison of Ansys and Experimental Stress Result for Outer surface of Ring Gear

The software stress values are closer to the experimental stress values and the stress values are increased with increased in input torque. The strain gauge position 1 shows the maximum stress induced in it because it is pasted in between the two bolting positions as shown in Fig. 10. Strain gauge position 3 is pasted exactly above the bolting position; therefore minimum stress is induced.

6.1 Experimental Rim Stresses for different angular positions of planet gears

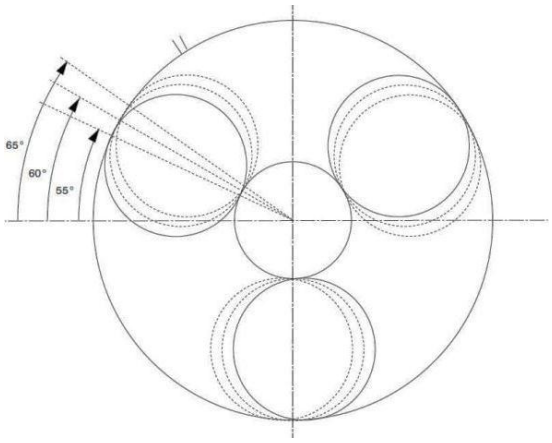

Fig. 11 Different positions of planet gear

Table 5 Experimental rim stresses for 65 deg of rotation

Angle(deg)	Weight (Kg)	Torque (Nmm)	Experimental Stress Results (N/mm^2)		
			Position 1	Position 2	Position 3
65	0.500	2910	0.0500	0.3000	0.0500
	1.000	5830	0.0900	0.6200	0.0800
	1.500	8750	0.1000	0.7600	0.0700
	2.000	11670	0.1300	0.8600	0.0400
	2.500	14590	0.1400	1.1200	0.0500
	3.000	17510	0.1400	1.1600	0.0400
	3.500	20420	0.1400	1.2000	0.0400

Experimental rim stresses are obtained by changing the output shaft rotation by 5° that means the rotation of planet gear with respect to horizontal axis as shown in Fig.11. As the position of the strain gauges are fixed at 120° on the outer surface of the ring gear therefore contact of the ring and planet gear vary as the rotation of the carrier takes place.

Fig. 12 shows that the stresses on the outer surface of the ring gear at three different positions, as strain gauge position 2 is exactly between the two bolting positions therefore it shows maximum stress induced at that position. Strain gauge position 1 and 3 are above the bolting position therefore it shows minimum stress induced as compared to position 2.

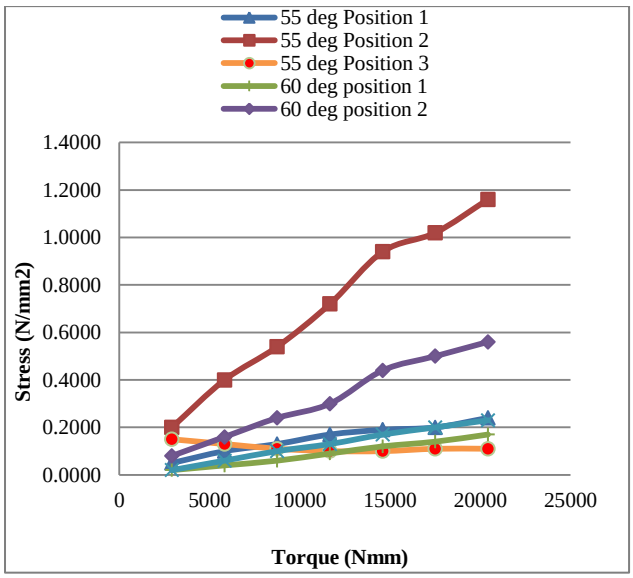

Fig. 12 Comparison of experimental stresses for different angular position

6.2. Ring Gear Stress along the thickness

Stresses in the ring gear are calculated along the thickness and the notations are used as shown in Fig. 11. The variation of stresses in rim along the thickness is shown in Fig. 13 which are validated with experimentally calculated values as shown in Table 6.

Fig. 14 shows the graph of stress distribution along the thickness of the ring gear which is closer to theoretical stress distribution as shown by Timoshenko.

As shown in Fig. 16 angular rotation Vs stresses induced on outer surface of the ring gear. In which maximum stress is developed where the teeth of planet and ring gear are in contact and the minimum stress is developed near the fixing bolt position.

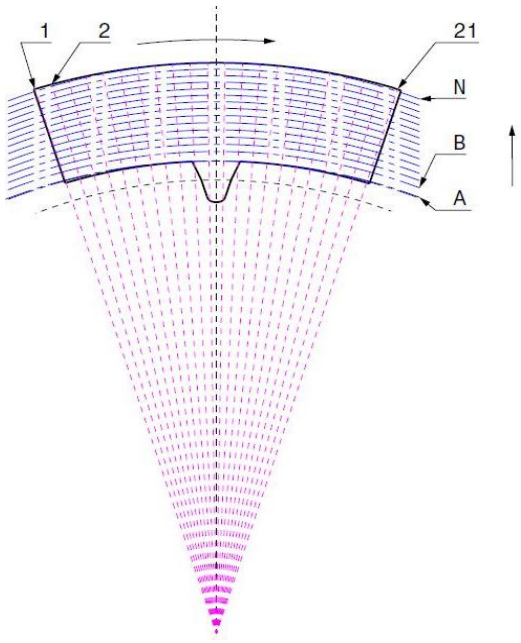

Fig.13 Rim thickness variation from A to N and angular variation from 1 to 21.

Table 6 Ring gear stress along the thickness

Sr.No	Rim Thickness (mm)	Stress (N/mm^2)
1	0	0.2565
2	2	0.1207
3	4	0.08241
4	6	0.05241
5	8	0.03087
6	10	0.02125
7	12	0.01393
8	14	0.01295
9	16	0.01567
10	18	0.01655
11	20	0.01511
12	22	0.01325
13	24	0.01057
14	26	0.01229

Table7 Ring gear stresses for different angular position

Sr. No.	Angular Rotation in deg	Outer Rim Stress N/mm^2
1	0	0.003633
2	2.25	0.00804
3	4.5	0.01532
4	6.75	0.0223
5	9	0.02159
6	11.25	0.01328
7	13.5	0.003361
8	15.75	0.008464
9	18	0.02659
10	20.25	0.05514
11	22.5	0.09263
12	24.75	0.13554
13	27	0.17112
14	29.25	0.1897
15	31.5	0.1837
16	33.75	0.155664
17	36	0.11205
18	38.25	0.05366
19	40.5	0.02455
20	42.75	0.04351
21	45	0.05088

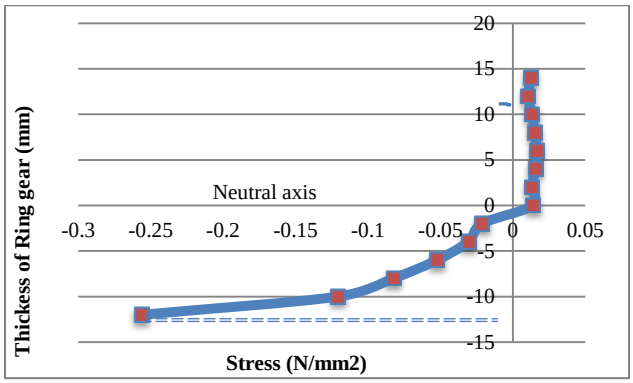

Fig.14 Ring gear stress along the thickness

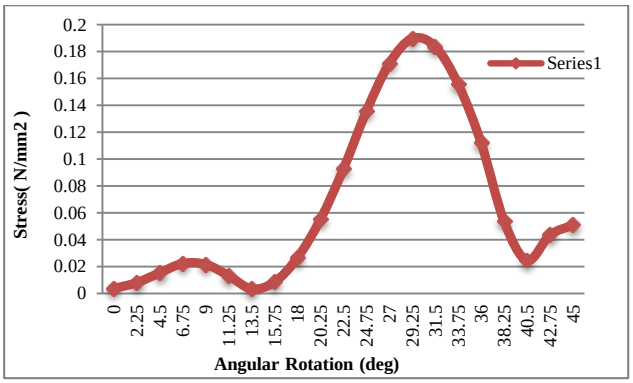

Fig. 16 Ring gear stresses for different angular position.

6.3 Ring Gear Stresses at Different Angular Position

The analysis is carried out on the sectional ring gear assembly as shown in Fig. 15, the boundary conditions are applied as mention in section 4.2, and stresses are measured on outer surface of the ring gear.

As shown in Fig. 16 angular rotation Vs stresses induced on outer surface of the ring gear. In which maximum stress is developed where the teeth of planet and ring gear are in contact and the minimum stress is developed near the fixing bolt position.

6.4 Bending Stresses of Ring Gear

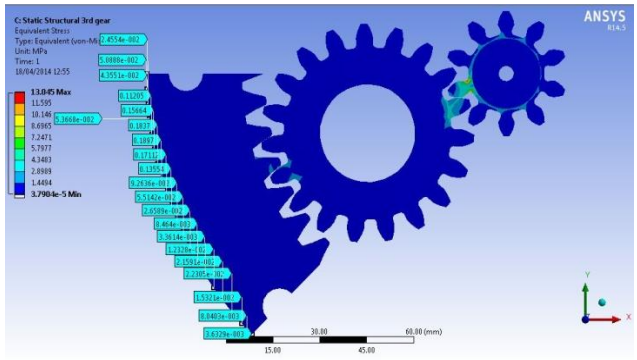

Fig. 15 Ring gear stresses on outer surface of rim

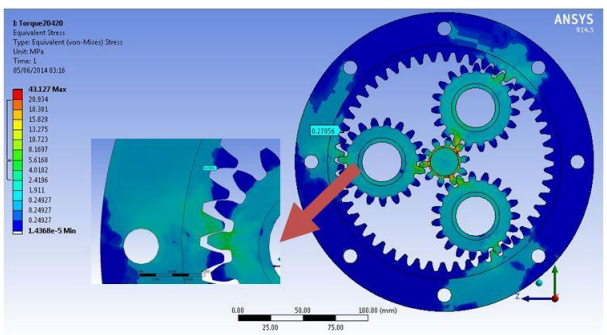

Fig. 17 Bending stress on ring gear tooth profile

Table 8 Comparison of FEM bending stress with experimental bending stress

Weight (Kg)	Torque(Nmm)	FEM Bending Stress (N/mm2)	Strain Indicator Reading	Multiplying Factor	Experimental Stress (N/mm^2)	% of error
1	5830	0.0581	0.12	0.5	0.06	3.1167
1.5	8750	0.0669	0.14	0.5	0.07	4.4714
2	11670	0.1137	0.24	0.5	0.12	5.2167
2.5	14590	0.1355	0.28	0.5	0.14	3.2143
3	17510	0.2055	0.44	0.5	0.22	6.5864
3.5	20420	0.2706	0.56	0.5	0.28	3.3714

The FEM analysis is carried out as discussed in section 4 and the same model is used to find out the bending stresses introduced in the ring gear tooth. The bending stress is measured at second teeth from the contact of the planet and ring gear. As shown in Fig. 17 the probe is used to select the required node point to find out the stress coming on that node.

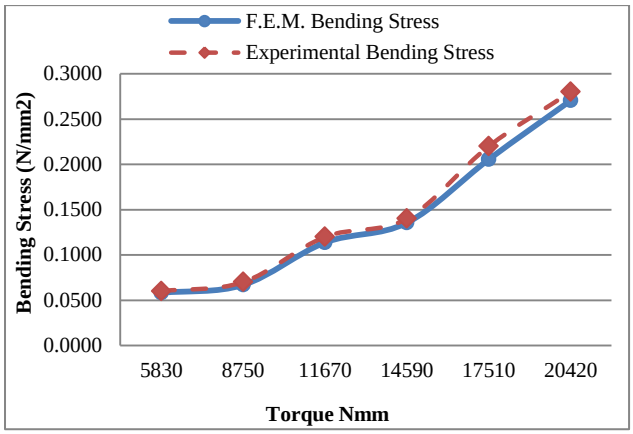

Fig. 18 Comparison of experimental and FEM ring gear bending stress.

Fig. 18 shows the comparison of experimental and FEM ring gear bending stress. As the input torque is increased the bending stress is also increased. Experimental bending stresses are closer to the FEM. bending stresses.

Conclusions

1. Experimental ring gear rim surface stresses are in good agreement with FEM results.
2. Stress variation across the thickness of the ring gear rim is estimated and validated by FEM results. The surface stresses on rim of ring gear at different angular positions are in good agreement with software results.
3. The maximum stresses on the outer surface of the ring gear are developed where the teeth of planet and ring gear are in contact and the minimum stresses are developed near the fixed bolt position.
4. Root stresses in ring gear are evaluated by software, as the torque on sun gear increases maximum stress increases and are compared with theoretically and experimentally.

References

Andrzej Kawalec, Jerzy Wiktor, Dariusz Ceglarek, (2006),Comparative Analysis of Tooth-root Strength Using ISO and AGMA Standard in Spur and Helical Gear with FEM-based Verification, *Journal of mechanical Design*, ASME, vol. 128, pp. 1141-1158.

M. Rameshkumar, G. Venkatesan, P.Sivakumar, (2010), Finite Element Analysis of High Contact Ratio Gear, *AGMA Technical Paper*, pp.1-12.

Miryam B. Sanchez, Jose I. Pedrero, Miguel Pleguezuelos,(2013), Critical stress and load conditions for bending calculations of involute spur and helical gears, *International Journal of Fatigue*, Elsevier, 48,pp.28-38.

Shuting Li,(2008), Effect of addendum on contact strength, bending strengthand basic performance parameters of a pair of spur gears, *Mechanism and Machine Theory*, Elsevier, 43, pp.1557-1584.

Takeshi Ishida, Teruaki Hidaka, TakahiroMikami, Hideharu Takizawa, (1986), Theoretical analysis of nominal stress in rim of planet gear, *Technology reports of the Yamaguchi University Yamaguchi University*, 3(5), 377-384, pp.377-384

Th. Costopoulos, V. Spitas, (2009), Reduction of gear fillet stresses by using one-sided involute asymmetric teeth, *Mechanism and Machine Theory*, Elsevier, 44,pp. 1524–1534

Niels L. Pedersen, (2010), Improving bending stress in spur gears using asymmetric gears and shape optimization, *Mechanism and Machine Theory*, Elsevier, 45, pp. 1707-1720

Seok-Chul Hwang, Jin-Hwan Lee , Dong-Hyung Lee, Seung-Ho Han, Kwon-Hee Lee, (2013) , Contact stress analysis for a pair of mating gears, *Mathematical and Computer Modelling*, Elsevier, 57, pp.40–49.

RaynaldGuilbault, Claude Gosselin, Louis Cloutier, Helical Gears, Effects of Tooth Deviations and Tooth Modifications on Load Sharing and Fillet Stresses, Journal of mechanical Design, ASME, 2006, vol.128, pp.444-456.

Darle W. Dudley, Handbook of Practical Gear Design, McGraw-Hill, 1986.

Timoshenko S.P., Strength of material, McGraw-Hill.